Macromolecules

Article

pubs.acs.org/Macromolecules

Ionic Conductivity in Polyelectrolyte Hydrogels

Honghao Li,[†] Aykut Erbaş,[‡] Jos Zwanikken,[‡,∥] and Monica Olvera de la Cruz*[,†,‡,§]

[†]Department of Applied Physics, [‡]Department of Materials Science and Engineering, and [§]Department of Chemistry, Department of Chemical and Biological Engineering and Department of Physics, Northwestern University, Evanston, Illinois 60208, United States

[∥]Department of Physics and Applied Physics, University of Massachusetts Lowell, Lowell, Massachusetts 01854, United States

ABSTRACT: Transport of ionic species in heterogeneous polymeric media is highly dependent on the charge distributions and interactions between mobile and immobile groups. Here we perform coarse-grained molecular dynamics simulations to study the ion dynamics in swollen polyelectrolyte gels under external electric fields. A nonlinear response of the ionic conductivity to an applied electric field, for field strengths that are comparable to the ionic coupling strength, is observed. This behavior correlates to a broadening of the ionic distribution around the polymer backbone under an increasing electric field. Also, we find that the weak-field ionic mobility in gels increases with density, which is opposite to the behavior of simple electrolytes. This relates to the mean coupling between charges that decreases in gels, but increases in simple electrolytes, with increasing density. These results provide more insights into the electric response of polyelectrolyte gels to support the development of applications that combine electric and mechanical properties of polyelectrolyte gels for energy storage, sensing, selective transport, and signal transfer.

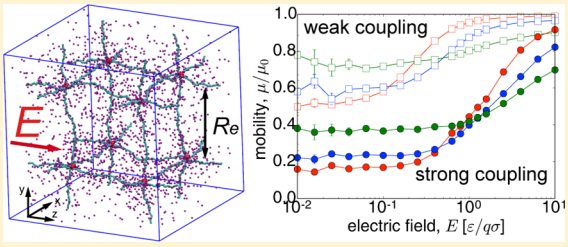

INTRODUCTION

Ionic transport in heterogeneous media on the microscale and nanoscale is of paramount interest for many applications including water desalination,[1,2] biomimetic systems,[3,4] and the potential for future generations of man-made devices, which can interface and be intrinsically compatible with biological tissues. An important type of heterogeneous medium is the polyelectrolyte gel.[5−11] These polymer networks are cross-linked polyelectrolyte chains with ionizable groups covalently bonded to the backbones. At specific conditions (e.g., pH, temperature), the ionized counterions dissolve into solvent as the only mobile charge species.

The unique property of polyelectrolyte gels as single-ion conductors has been used to synthesize ion-selective membranes. In electrodialysis, one of the common techniques to produce drinking water in addition to reverse osmosis and nanofiltration, ions are selectively transported from one solution (diluted) to another solution (concentrated) through ion-exchange membranes under an electric potential difference. These membranes are anionic (cationic) polyelectrolyte gels with positively (negatively) charged groups, which reject positively (negatively) charged ions and allow negatively (positively) charged ions to flow through. Polyelectrolyte gels have also been facilitated in the area of soft ionic devices, such as ionic diodes,[12−14] ionic transistors,[15−18] and ionic conductors.[7,19] One example is the polyelectrolyte diode composed of two hydrogel layers doped with oppositely charged polyelectrolytes; the oppositely charged counterions produce a nonlinear current response as a rectifying junction at the interface.[13,14] Not surprisingly, in almost all field driven processes, mobility of ionic species in gels depends on the distribution of the charged and uncharged groups, electrostatic coupling strength (e.g., polarity of the solvent), and molecular details of the background network.

Experimentally, ionic conductivity of polyelectrolyte gels has been measured in various conditions.[20−24] The concentration-dependent ionic conductivity of polyelectrolyte gels is reported to differ from those of polyelectrolyte solutions or binary electrolytes.[20,25] In electrolyte solutions, increasing concentration leads to a decrease in molar conductivity, while no distinct concentration dependencies of molar conductivity were observed for gels. In addition, the ionic conductivity in polyelectrolyte gels has been reported to depend on cross-linking density (i.e., the average molecular weight between cross-linkers).[20,23,26] This hints that topology of these gels at the nanometer scale is of paramount importance in altering membrane function. Hence, further design of such systems requires theoretical determination of interactions between ionic species and the gel network and of the effect of accessible parameters.

In this study we use coarse-grained molecular dynamics (MD) simulations to investigate the ion dynamics in polyelectrolyte gels under external electric fields. We find a nonlinear response region, where the molar ionic conductivity of polyelectrolyte gels increases with external fields. The counterion redistribution under electric fields is proposed as the underlying mechanism. We also show that the ionic conductivity can be modulated by changing the polyelectrolyte network density particularly in the weak-field regime. The simulations reveal that the mobility increases as the density of

Received: June 14, 2016
Revised: November 1, 2016

DOI: 10.1021/acs.macromol.6b01276
Macromolecules XXXX, XXX, XXX−XXX

charged monomers increases when the electric field is small, where linear response theory can be applied. Above a critical field strength, the linear response regime breaks down and then the mobility decreases as the concentration of monomers increases. This is observed well before the saturation value. Note that there is no obvious reason for the existence of two concentration-dependent mobility behaviors. A qualitative theory based on a field-induced weakening of binding energies can qualitatively describe the mobility of counterions for the range of external fields considered here. Our results also underline an essential difference between the ionic response in simple electrolyte solutions and that in polyelectrolyte gels. These results could be extremely important in many new areas of research given the large number of new applications of polyelectrolytes gels in energy storage where there is a need to understand diffusivity and mobilities in different regimes (slow or rapid charging with electric fields and discharging by diffusion).[27−30]

METHODS

Simulation Model. Figure 1a illustrates the unit cell of a defect-free isotropic cubic polyelectrolyte network that is used in the simulations. The polymer segments connecting two network nodes are modeled by bead−spring chains composed of N monomers. The steric and bonded interaction between monomers are calculated by the Lennard-Jones (LJ) and FENE (finite extension nonlinear elastic) potentials in the forms of

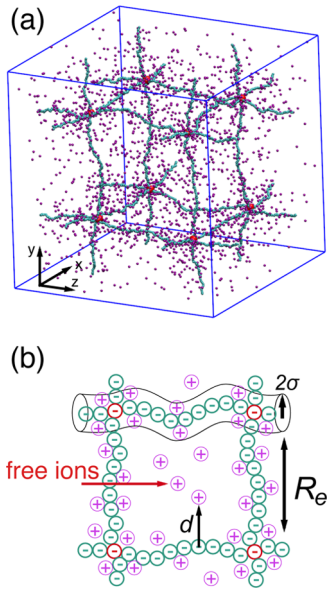

Figure 1. (a) Snapshot depicting the unit lattice of a $N = 100$ isotropic polyelectrolyte network structure. Monomers and counterions are denoted by cyan and purple spheres, respectively. Each cross-linking node (drawn as oversized red spheres for illustration purposes) is attached by six polyelectrolyte chains, each of which has N monomers. Unit cell box in simulation typically has $4 \times 4 \times 4$ cross-linking nodes ($2 \times 2 \times 2$ shown here). (b) Illustration of the cell parameter that is used to determine condensed ion distributions. The distance from chain d is defined by the distance between an ion and its nearest monomer. The ion is considered as condensed ion when $d \leq 2\sigma$.

$$U_{LJ}(r) = \begin{cases} 4\epsilon\left[\left(\frac{\sigma}{r}\right)^{12} - \left(\frac{\sigma}{r}\right)^{6} + \frac{1}{4}\right] & \text{for} \quad r < r_c \\ 0 & \text{for} \quad r \geq r_c \end{cases}$$

$$U_F(r) = \begin{cases} -\frac{1}{2}k_F r_F^{\,2} \ln\left[1 - \left(\frac{r}{r_F}\right)^2\right] & \text{for} \quad r < r_F \\ \infty & \text{for} \quad r \geq r_F \end{cases}$$

Here the LJ potential is shifted at the cutoff radius $r = r_c$ to obtain a continuous potential profile. σ is the monomer diameter (LJ units).[a] Good solvent conditions are modeled by $r_c = 2^{1/6}\sigma$ and $\epsilon = 1k_BT$, leaving only the repulsive part of the interactions. This potential is employed for both the mutual chain−counterion and counterion−counterion excluded volume interactions. For the FENE bond, the parameters are set to $k_F = 10.0k_BT/\sigma^2$ and $r_F = 1.5\sigma$.[31] Periodic boundary conditions are applied in all direction in the simulation box. A typical cubic simulation box contains $4 \times 4 \times 4$ cross-linking nodes in xyz directions. The sizes of simulation box for different gels are in the range of $50\sigma-200\sigma$.

The sizes of all counterions and backbone monomers are equal to 1σ. Each counterion has a unit charge of $q = +1e$, while each backbone monomer of N-mer chains bears a unit charge of $q = -1e$. Initially, counterions are added at random positions in the periodic simulations box. Because of the macroscopic requirements of electroneutrality, the number of counterions is set equal to the total number of charged backbone monomers. The short-range pairwise Coulomb interaction between two charges is $U_{Coul}(r) = \epsilon l_B q_i q_j / r$, where the Bjerrum length is $l_B = e^2/(4\pi\epsilon_0\epsilon_s\epsilon)$. Here e is the unit charge; ϵ_0 and ϵ_s are the permittivity of the vacuum and the solvent, respectively. The Bjerrum length is defined as the distance, at which two unit charges have an electrostatic interaction energy equivalent to thermal energy k_BT. As an example, for water $l_B \approx 7$ Å $= 1\sigma$ and is roughly equal to four adjacent carbon−carbon bonds and the hydrated ion diameter of simple electrolytes such as Na^+. For less polar solvents such as n-propyl alcohol at 40 °C, $l_B \approx 35$ Å $\approx 5\sigma$.[32] The long-range Coulomb interaction is calculated via the PPPM algorithm,[33] with a force accuracy of 10^{-4}. The cutoff distance that determines the short- and long-range scheme in simulations is chosen to optimize the computation time between real and K-space. Typically, the range of the electrostatic cutoff distance ranges $8\sigma-20\sigma$ depending on the size of the system.[34] Isothermal−isobaric (NPT) ensemble for implicit solvent is used to allow swelling of gels to obtain the equilibrium volume of the system ($V_{eq} = V(P=0)$) prior to nonequilibrium simulations.[35]

The nonequilibrium simulations are conducted by applying a constant external electric field on each charged particle (i.e., the external force per monomer is $\mathbf{F}_{ext} = q\mathbf{E}$). The external electric fields are in the range of $10^{-2}-10^{1}\epsilon/q\sigma$ and in the z-direction ($\mathbf{E} = E\hat{z}$).

The molecular dynamics simulations are performed using LAMMPS software packages.[36] The Langevin equation of motion are solved to iterate velocities and coordinates of particles. To keep the temperature constant in all the simulations, a Langevin thermostat scheme is applied with a damping parameter of $\gamma = 0.1\tau^{-1}$, where the reduced time unit is $1\tau = \left(\frac{\epsilon}{m\sigma^2}\right)^{1/2} t$. Throughout the thermostatting process, each bead experiences a dissipative force of $\mathbf{F}_i^D = -\gamma\mathbf{v}_i$, where $\mathbf{v}_i$ is the velocity of ith bead, and a random force, $\mathbf{F}_i^R$, which satisfies the fluctuation−dissipation theorem.[37]

Since the network chains are not entangled (i.e., they are highly stretched), a Rouse type of relaxation time $\tau_N \sim N^2$ is enough for N-mer network chains. For $N = 100$ gels, typically $10^4\tau$ (10^6 time steps with $\Delta t = 0.01\tau$) is an acceptable relaxation time.[38] Following the relaxation, in the field driven cases, an additional 2×10^7 time steps ($\Delta t = 0.005\tau$) are run for the data used in the analysis. The statistical errors of time-series data are analyzed by using block averages as detailed in refs 39 and 40. Error bars that are of the order of the symbol size or smaller are not shown in the figures.

Mobility Calculations. The average drift velocity of all counterions relative to the polyelectrolyte network under the field is used to calculate the average mobility of counterions, regardless of their relative positions

DOI: 10.1021/acs.macromol.6b01276
Macromolecules XXXX, XXX, XXX−XXX

$$\mu = \frac{\langle v_{ci} \rangle}{qE} \tag{1}$$

where the angular brackets $\langle ... \rangle$ refer to averaging over all the ions and time frames. The mobility of counterions can be related to the molar conductivity by $\Lambda = q\mu$. Additionally, the diffusion coefficient of counterions at vanishing fields (i.e., $D \equiv k_B T \mu(E \to 0)$) is calculated from the mean-square displacement of counterions by

$$D = \lim_{t \to \infty} \frac{\langle [\mathbf{r}(t) - \mathbf{r}(0)]^2 \rangle}{6t} \tag{2}$$

where $\mathbf{r}(t)$ is the position vector of an ion at time t.

In addition, by using trajectories we calculate the position-dependent mobility for the ith counterion, μ_i, located at d_i, where d_i is the distance between the ith counterion and the closest chain monomer (Figure 1b). The mobilities are binned with respect to their distances to the chains. The total number of bins is 100, and the maximum d_i considered is $\approx R_e/3$ for all cases, where R_e is the network-chain end-to-end size.

To calculate the integrated distribution for the counterions near the network chains, the counterions whose distances obey $d_i < d$ are determined, and their population is plotted as a function of d.[35,41]

RESULTS AND DISCUSSION

Polyelectrolyte Gels in the Absence of External Electric Field. To systematically reveal the effect of the external field in the next section, we first consider the equilibrium distribution of charges and related transport properties in gels at vanishing electric fields. In a polyelectrolyte gel, the balance between the osmotic pressure of ionized counterions and the elastic response of the network chains leads to highly stretched network chains. The scaling theory gives the average end-to-end distance of the network chains as $R_e \simeq N\sigma$ for a finite charge fraction (i.e., $f > 0$).[42,43] In the simulations, where we have strongly charged polyelectrolyte chains (i.e., $f = 1$), $R_e \sim N$ for various electrostatic strengths and for $N \gg 1$ (Figure 2a). As the electrostatic strength (Bjerrum length) is increased, the polyelectrolyte gels are less swollen due to the increased localization (condensation) of the counterions onto the network chains[44] (Figure 2a).

An estimate for the fraction of counterions condensed onto the chains (nonfree ions) f_{CI} can be obtained by counting the ions confined in cylindrical cells of radius 2σ around each chain[45] (see Figure 1b for the schematic definition). The fraction of condensed ions is much higher for strong electrostatic coupling as expected (Figure 2b). However, independent of the electrostatic coupling, the fraction of condensed counterions approaches plateau values only for very dilute polyelectrolyte gels (i.e., $N > 100$) (Figure 2b).

According to Manning's theory of condensation,[26,46] a single strongly charged and infinitely long charged rod attracts oppositely charged counterions to reduce its line charge density. Similar phenomena in polyelectrolyte gels have been reported in previous simulation studies.[35,44] The simplified Manning model predicts the fraction of condensed counterions as $f_{CI} = 1 - 1/\xi$ for $\xi > 1$, where the Manning parameter is $\xi = l_B/\sigma$ as in our case with $f = 1$. For $l_B = 1\sigma$ and $l_B = 5\sigma$, the predicted Manning values, $f_{CI} \to 0$ and $f_{CI} = 0.8$, respectively (dashed line in Figure 2b). Our results suggest that the Manning picture is still qualitatively valid for ion distributions in gels in the dilute limit. A more accurate method indeed uses the inflection point based on Poisson–Boltzmann theory to estimate the counterion condensation around single chains[45,47,48] yet cannot be easily applied to arbitrary geometries such as networks in our simulations.

The transport properties of counterions are related to the fraction of condensed ions since electrostatic forces exerted on the counterions depend on their position relative to the stretched network chains. In Figure 3a, we show the diffusion coefficient calculated over all counterions as a function of N for

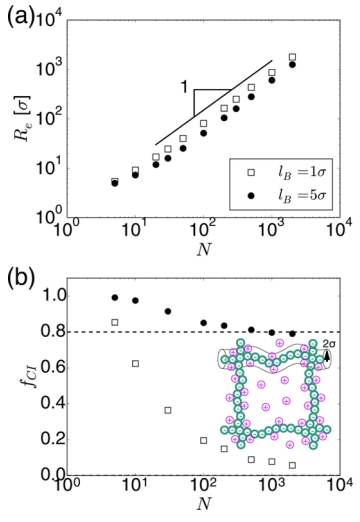

Figure 2. (a) Average end-to-end sizes of the polyelectrolyte network chains R_e as a function of monomer number between two cross-links N for both $l_B = 1\sigma$ and 5σ cases. A linear reference line is shown to guide the eye. (b) Fraction of condensed counterions f_{CI} at zero external electric field. All ions within a distance of 2σ around the backbone chains are considered as condensed. Note that as $N \to \infty$, the counterion condensation ratio approaches the Manning theory (dashed line).

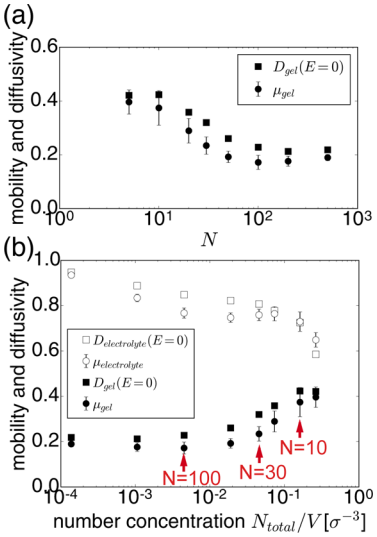

Figure 3. (a) Linear-response mobilities μ and equilibrium diffusivities D of counterions in gels as a function of N, for an electrostatic strength of $l_B = 5\sigma$. (b) Comparison of μ and D of counterions in gels and 1:1 simple electrolytes with identical concentrations. Note concentration is lower for gels with larger N. Gels with $N = 500$ to 5 are studied here, where $N = 100$, 30, and 10 are marked for clarity. The diffusion coefficients are calculated via mean-square displacement of counterions (MSD) in eq 2 at zero field, whereas the mobilities are calculated via eq 1 at $E = 0.1\epsilon/q\sigma$. All the mobilities and diffusivities are normalized by the Langevin damping parameter $\mu_0 = 1/\gamma$.

DOI: 10.1021/acs.macromol.6b01276
Macromolecules XXXX, XXX, XXX−XXX

$l_B = 5\sigma$. Interestingly, for larger values of N (i.e., the monomeric concentration c is lower, see Figure 3b), the diffusion coefficient of the counterions decreases. This hints that the high counterion mobilities cannot be explained by a simple condensation model since one would expect that more localized ions would lead to slower transfer coefficients. We will discuss counterion distribution profiles in more detail in the next sections. Figure 3b also compares the diffusivity of ions in the polyelectrolyte networks to that of 1:1 binary electrolyte solutions at the identical ionic concentrations. Unlike polyelectrolyte gels, in the electrolyte solution, diffusion of ions is faster for lower concentrations, as also observed experimentally.[20]

At lower electrostatic strengths (i.e., $l_B = 1\sigma$), although the trend in the diffusion coefficient is similar to the $l_B = 5\sigma$ case, the difference in mobilities at low and high concentrations is weaker (data not shown). This again indicates the dependence of averaged transport coefficients on the position of ions with respect to the backbone chains since, for $l_B = 5\sigma$, ions are more condensed onto the network chains.

The equilibrium charge distribution and diffusion behavior in polyelectrolyte gels that we discuss so far is expected to be altered under external electric fields. In the following section, we discuss how the applied field alters the charge distribution and, in turn, the mobility of mobile counterions in polyelectrolyte gels.

Effect of External Fields. Figure 4 shows counterion mobility in various polyelectrolyte gels with $N = 10$, 30, and

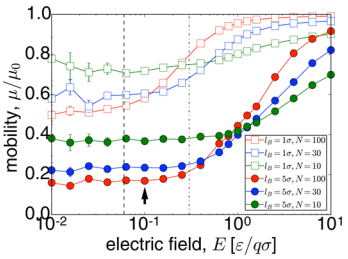

Figure 4. Mobility of counterions for various gels under external electric fields for both $l_B = 1\sigma$ and $l_B = 5\sigma$. All the mobility values are rescaled by the Langevin damping parameter $\mu_0 = 1/\gamma$. Arrow indicates the value of the electric field ($E = 0.1\epsilon/q\sigma$) that is used in Figure 3. Notice that this field is within the linear-response regime. The dashed lines are guide to the eye in order to indicate the onset of nonlinear regime for $N = 100$ gels.

100 for Bjerrum lengths $l_B = 1\sigma$ and 5σ. To compare various cases on a single plot, all mobilities are normalized by their bulk value $\mu_0 = 1/\gamma$, where γ is the Langevin friction term. Based on the data in Figure 4, the mobility of counterions in polyelectrolyte gels under the external electric field E can be discussed under three regimes:

i. Linear-Response Regime. In this regime, the electric field is not strong enough to alter the equilibrium distribution and the related transfer properties of charge carriers significantly. The mobility remains constant as long as the external electric fields is weaker than the electrostatic coupling between backbone charges and counterions (i.e., $E < E^* \equiv \epsilon l_B/\sigma^2$) (Figure 4). This regime corresponds to weak perturbations (e.g., Ohm's law is valid).

The linear-response behavior can also be seen in Figure 3, where we compare the mobility values obtained at an electrical field strength within the linear regime, $E = 0.1\epsilon/q\sigma$ (filled spheres in Figure 3), to the equilibrium diffusion coefficients (filled squares). The diffusion coefficients are calculated via eq 2 and related to the mobilities with the Einstein relation, $D = k_BT\mu$. The linear-response mobility indeed converges to the equilibrium diffusion coefficients within error as $E \to 0$ in Figure 3.

In Figure 4, within the linear-response regime, the gels composed of shorter network chains exhibit slightly larger mobilities in accord with the data in Figure 3. To further reveal the effects of counterion clouds near network chains, in Figure 5a we show the integrated distributions of counterions around

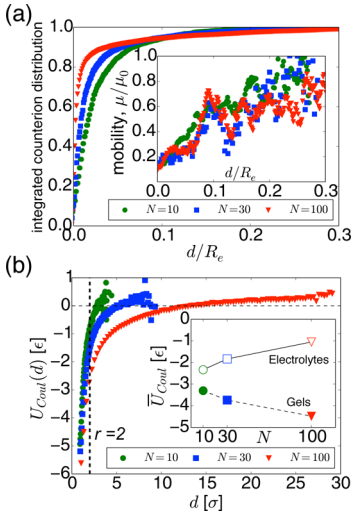

Figure 5. (a) Integrated ion distributions for various polyelectrolyte networks. The distance from chain d is normalized by the end-to-end distance R_e. Inset shows mobility of ions as a function of their distance from chains at $E = 0.1\epsilon/q\sigma$ with $l_B = 5\sigma$. A moving average is performed to improve the noisy raw data. (b) Calculated electrostatic energy of counterion as a function of its distance to chains. Inset shows average Coulomb energy per counterion ($\bar{U}_{coul} = \sum_i U^i_{coul}/N_{ions}$) in various gels and 1:1 binary electrolytes at identical ionic concentrations at $E = 0.1\epsilon/q\sigma$.

the network chains as a function of the rescaled distance from the nearest chain d/R_e. The strength of electric field is $E = 0.1\epsilon/q\sigma$ for all cases. In Figure 5a, the data for $l_B = 5\sigma$ are specifically chosen to demonstrate the effect of condensation more clearly. In Figure 2, the condensation is calculated by considering the counterions within a cylindrical region around each network chain. According to this calculation, the condensation is more marked for system with short chains, since the relative volume of the cylindrical region is larger. However, the counterion clouds near the chains are relatively more extended in the gels composed of short chains due to mutual attraction by the backbone charges of the neighboring chains (Figure 5a). Indeed, the average mobility of counterions is higher if they are away from the network chains as can be seen in the inset of Figure 5a. Despite the noise in the data due to thermal fluctuations, the closer the counterions are to the networks chains, the slower they move. Hence, if the counterions are more scattered in the gel, the average mobility is larger (Figure 5a).

The extended ionic clouds near the polyelectrolyte network chains manifest themselves also in the electrostatic potential distribution. The position-dependent electrostatic potential is calculated by computing the electrostatic energy of each ion

DOI: 10.1021/acs.macromol.6b01276
Macromolecules XXXX, XXX, XXX−XXX

and averaged over many time steps. The results are shown in Figure 5b. Near the chains (i.e., $d/R_e \to 0$), deep potential wells are common in all networks. Away from the chains, the potentials decay to zero (Figure 5b). At intermediate distances, the Coulomb potential is stronger in gels with longer chains. This indicates that for a counterion located near, say $N = 100$ network, escaping from the potential requires higher forces compared to that in a $N = 10$ network. Combining these results with the counterion distributions in various polyelectrolyte networks shown in Figure 5a, the decrease in ionic mobility with increasing size of network chains in the linear-response regime can be related to distribution of counterions in dilute gels.

ii. Transition Regime. The linear-response regime ends at around $E \simeq E^*$, and the transition regime, where the mobility increases with increasing strength of electric field, sets in (Figure 4). Linear polyelectrolyte solutions also exhibit similar nonlinear response to external electric fields.[49] In Figure 4, the threshold electric field strengths for $N = 100$ gels are denoted by two dashed lines for $l_B = 1\sigma$ and $l_B = 5\sigma$ cases, respectively, and by definition $E^*_{l_B=5\sigma}/E^*_{l_B=1\sigma} = 5$.

To address the underlying mechanism of the nonlinear mobility of counterions at $E > E^*$, the microscopic distribution of counterions is investigated. Indeed, strong electric fields are known to reduce the number of condensed counterions near the charged chains.[45,49] In Figure 6a,b, we show the integrated distributions of counterions around the chains of the $N = 100$ network at various electric field strengths. The values of the electric field correspond to both linear and nonlinear regimes (Figure 4). For both $l_B = 1\sigma$ and $l_B = 5\sigma$ cases, at vanishing electric fields, the distributions are weakly affected by the external field as expected. However, at $E > E^*$ the counterion distributions are broader as a result of the counterions departing away from the network chains. This can be seen more clearly in the 2D concentration profiles shown in Figure 6c for two different external fields, $E = 0.1\epsilon/q\sigma$ and $E = 1\epsilon/q\sigma$. At the higher field, more ions occupy spaces between the network chains (notice the light and darker blue regions in Figure 6c).

Saturated Regime. In this regime, due to the strong external field ($E \gg E^*$), most of the condensed ions are stripped off the network chains and dragged by the field. Indeed, when E is strong enough, the resulting mobility is expected to be independent of network properties and electrostatic coupling for highly swollen gels. The mobility of counterions becomes independent of the applied field and approaches its bulk value $\mu \to \mu_0 = 1/\gamma$ (Figure 4). However, we should note that in the cases of dense gels (i.e., when the end-to-end distance does not obey the scaling $R_e \sim N$),[50] the counterion diffusion can be coupled to chain motion. Thus, the final saturation values can be a function of cross-linking density. Interestingly, the higher weak-field mobility observed for shorter network chains are reversed at the saturation regime, since physical hindrance due to the network chains is weaker in dilute gels (i.e., $N \gg 1$).

The detailed analysis of the counterion mobility and related concentration profiles suggests that the main contribution to the mobility in polyelectrolyte gels are from uncondensed (free) ions that can move through the network structure. Indeed, there is an excellent correlation between the fraction of free ions and the mobility for a wide range of external fields as shown in the insets of Figure 6a,b. The fraction of the free counterion as a function of external field overlaps with mobility

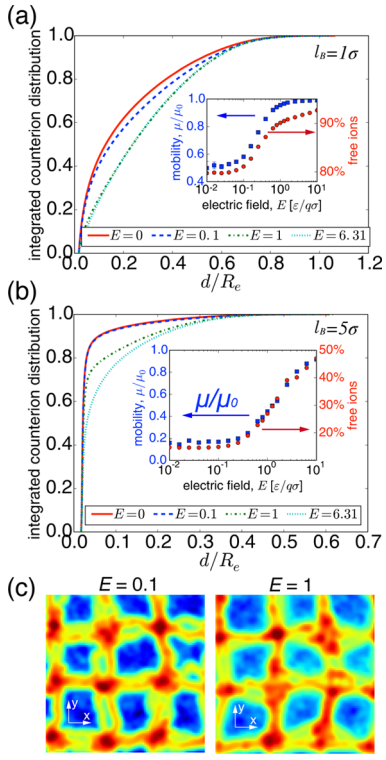

Figure 6. Integrated ion distribution around the chains of $N = 100$ polyelectrolyte networks for various external electric fields (a) $l_B = 1\sigma$ and (b) $l_B = 5\sigma$. The distance is normalized by the end-to-end distance R_e. Insets show mobility and number of free ions on a single plot. Blue squares denote the mobility values with respect to left y-axis, while red dots denote the fraction of free ions with respect to right y-axis. (c) 2D plots of counterions−concentration profiles are shown for $E = 0.1\epsilon/q\sigma$ (left) and $E = 1\epsilon/q\sigma$ (right); the external field is in the z-direction. The red regions refer to high local concentration of counterions around the network chains, whereas blue color refers to the low local concentration.

data remarkably well. Thus, the mobility can be expressed as the sum of contributions from the free and condensed ions as

$$\mu = \mu_{nf} f_{CI} + \mu_{free}(1 - f_{CI}) \quad (3)$$

where μ_{free} is mobility of free ions and μ_{nf} is mobility of condensed ions. As a simple estimate, in gel with $N = 100$, the fraction of condensation is $f_{CI} \simeq 0.8$ for $l_B = 5\sigma$ and $E = 0.1\epsilon/q\sigma$. Thus, eq 3 gives the mobility $\mu \simeq 0.2\mu_0$, which qualitatively agrees with simulation results. However, eq 3 is less accurate for weak electrostatic strengths, e.g., $l_B \approx 1\sigma$, since a distinction between "condensed" and "free" ions is hard to establish due to weaker interactions (which are of the order of the thermal energy) between the ions and the backbone charges.

Comparison: Simple Electrolytes versus Polyelectrolyte Gels. In 1:1 electrolytes in the dilute limit, according to Debye−Huckel theory, the molar conductivity Λ (which is proportional to diffusivity) decreases linearly with the square root of concentration, $\Lambda = \Lambda^0 - K\sqrt{c}$ (Kohlrausch's law), where K is a constant and Λ^0 is the molar conductivity at infinite dilution (or limiting molar conductivity). Accordingly, a single diffusing ion feels a drag friction due to the surrounding ionic atmosphere of oppositely charged ions. The drag force increases with increasing concentration. Thus, the ion diffusivity decreases with increasing concentration. In contrast,

DOI: 10.1021/acs.macromol.6b01276
Macromolecules XXXX, XXX, XXX−XXX

the ion diffusivity in polyelectrolyte gels increases with increasing concentration (Figure 3).

Note that simple electrolytes also have an underlying potential landscape, just like the gels, which in simple electrolytes is responsible for Kohlrausch's law. Interestingly, Kohlrausch's law is not observed by constraining one of the charged components to a flexible chain (in polyelectrolyte gels).

A scaling argument can be made to invoke the difference between simple electrolytes and PE gels. In electrolytes, the average distance between two ions in solution can be estimated as $\sim c^{-1/3}$, where c is the concentration. Hence, the average distance decreases with increasing concentration (assuming no charge pairs are formed). This results in stronger repulsions between like-charged ions and stronger attractions between oppositely charged ions. The inset of Figure 5b compares the average Coulomb energy per counterion in a 1:1 electrolyte solution to that in various gels at $E = 0.1\epsilon/q\sigma$, regardless of the ion positions. For the electrolytes, the absolute value of the Coulomb energy increases with increasing concentration. In contrast, for polyelectrolyte gels, the absolute value of the Coulomb energy decreases with increasing concentration. This behavior indicates an essential difference in ion distributions, which results in different ion dynamics in electrolytes and polyelectrolyte gels.

Ion Asymmetry and Hydrodynamics. In the simulations the sizes of all counterions and backbone monomers are equivalent. However, the steric interactions of counterions or solutes with the background network can alter the transfer properties.[51,52] Indeed, asymmetric steric interactions in ionic systems are known to change the charge−charge correlations.[53] In the gels considered here, the main effect is due to the free ions. Therefore, we expect that any asymmetry in ionic size can mostly change the threshold electric field for the onset of the nonlinear regime, while quantitatively the behavior of the mobility under external fields should be conserved.

Hydrodynamic effects are important in polyelectrolyte electrophoresis studies[45] and high concentration systems. According to previous studies,[54] hydrodynamic effects cause an approximate 2% difference of Na^+ diffusivity at a concentration of 0.25 M. In our study, only dense gels with $N \leq 10$ have a comparable counterion concentration ~0.25 M. Therefore, in the Langevin thermostat scheme applied here, hydrodynamic interactions between the monomers are not considered. Since the free counterions are far apart from each other in the dilute gels, we anticipate that hydrodynamic effects will not change the results qualitatively as long as the gels are swollen. In the calculations of the mobilities, we use the velocities of ions with respect to less mobile network chains. Adding hydrodynamics can slow down the ions particularly in the linear regime (i.e., weak fields), but overall our observations and related regimes will hold.

Theoretical Arguments for Mobility. In order to rationalize the behavior of the mobility from a different perspective, we develop a theoretical model to refine eq 3 and the notion of "free" and "condensed". We assume simple reaction equilibria, set by reaction constants K_i, connected to different states i of an ion. This rate constant is calculated from a single-ion partition function that depends on a mean binding (Gibbs) energy $\Delta G(E)$, depending on the external field E, and a volume V in which a single ion interacts with a site on the backbone.

$$K_i = V_i e^{\Delta G_i(E)} \tag{4}$$

In addition, we distinguish three regions: (1) the region where the ions are "free" ($\Delta G_1 = 0$), (2) the region where the ions are close to the chain but still mobile ($\Delta G_2 \sim 1k_BT$), and (3) the region where the ions are condensed and immobile ($\Delta G_3 \gg 1k_BT$). The number of ions in each region, n_i, is determined by a reaction equilibrium:

$$n_i = n\frac{K_i}{K_1 + K_2 + K_3} \tag{5}$$

We use an equation similar to eq 3 to estimate the total mobility, but now with three states for ions, corresponding to the three regions. Before we can make a comparison to the simulation results, many assumptions are required about the scaling behavior of V_i (the volume of region i) and the mean free energy of binding, and in principle also the mobility in region 2, although this parameter appeared of little influence. The predictions of the model depend sensitively on these assumptions, especially on the scaling behavior of V_i and $\Delta G_i(E)$ and also on the input parameters. However, regardless of the specific assumptions, we find general trends that largely coincide with the simulation results, namely, that the mobility increases with increasing field E because a larger E shifts the reaction equilibria in favor of region 1 (the "free" region), with a transition in the region where E has the same order of magnitude as the Coulomb pair interaction. The remarkable behavior in Figure 4 at small electric fields is in contrast, only predicted for rather specific assumptions. An important, but not sufficient, assumption is that ΔG in a dilute gel need to be larger than in a more dense gel. That is ions stick more strongly in dilute networks. This assumption is confirmed by the simulation results in Figure 5b. The results are shown in Figure 7, under the assumption that the length of the chains scale linearly with N, and ΔG decreases linearly with E, for $l_B = 5$:

$$\Delta G_i(E) = \Delta\phi_i - E \quad (\Delta\phi_i > E) \tag{6}$$

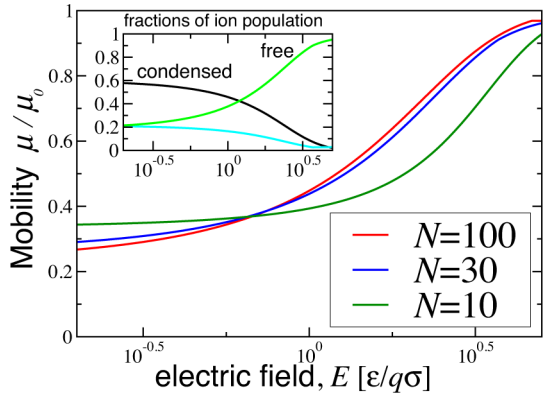

Figure 7. Mobility as a function of the applied electric field. The mobility increases with the electric field as the reaction equilibria shift toward the region where ions move freely (i.e., ions break free from the gel backbone). The contrast in the mobility is larger for dilute gels ($N = 100$). Under specific assumptions, the (relative) mobility at zero field is lower in dilute gels than the more dense gels. The simulations were required to confirm these assumptions and to show the same qualitative trend without these assumptions. The inset shows the fraction of the ion population in each of the three regions as a function of E, for $N = 30$.

DOI: 10.1021/acs.macromol.6b01276
Macromolecules XXXX, XXX, XXX−XXX

The drop in the average electrostatic potential $\Delta\phi_i$ in region i is estimated from a Poisson−Boltzmann theory, and $\Delta G_i = 0$ for $\Delta\phi_i < E$. From the perspective of this model we can draw two main conclusions. First, the nonlinear response can be rationalized as a general consequence of ions breaking free from the polymer backbone, which are being less impeded by the interactions with the polymer chains as the electric field increases. Second, we conclude that the density dependence of the mobility at low electric fields is not easily captured in a simple model and only reproduced under very specific assumptions for the scaling behavior of the gel volume and the binding energy of the ions. These assumptions are in line with the simulation results in the previous section. However, considering the simplifications in our theoretical models, and the number of unknown parameters, the molecular dynamics simulations are necessary for conclusive results. The model highlights qualitative trends and suggests conditions for the required scaling behavior of the binding energy and gel swelling.

CONCLUSION

We have analyzed the ion dynamics in polyelectrolyte gels by using molecular dynamics simulations and invoked theoretical models to rationalize the results. Regardless of the gel characteristics, we find a nonlinear response of the conductivity to an applied electric field for field strengths that are comparable to the ionic coupling strength. This behavior correlates to a broadening of the ionic distribution around the polymer backbone under an increasing electric field. The weak-field mobility for dilute gels can be directly estimated from the fraction of free ions, using Manning's theory, if the ionic coupling is larger than the thermal energy, $l_B/\sigma > 1$. For dense gels, the mobility is not easily estimated due to the complicated interplay of Coulomb interactions and steric repulsions. We find that the ion mobility in dilute gels shows a larger transition than in denser gels, and we connected the behavior to a larger binding energy of the ions to the polymer backbone. Remarkably, we find that the weak-field ion mobility in polyelectrolyte gels increases with increasing concentration, which is opposite to the behavior observed in simple electrolytes. This is related to the mean coupling between charges, which decreases in polyelectrolyte gels and increases in simple electrolytes, with increasing concentration. These results provide more insights into the electric response of polyelectrolyte gels to support the development of applications that combine electric and mechanical properties of polyelectrolyte gels for energy storage, sensing, selective transport, and signal transfer.

AUTHOR INFORMATION

Corresponding Author

*E-mail: m-olvera@northwestern.edu (M.O.d.l.C.).

Notes

The authors declare no competing financial interest.

ACKNOWLEDGMENTS

H.L. thanks Yufei Jing for his code for calculating electrostatic interactions. We thank Mykola Tasinkevych for valuable discussion. This work was supported by the Center for Bio-Inspired Energy Science (CBES), which is an Energy Frontier Research Center funded by the U.S. Department of Energy, Office of Science, Office of Basic Energy Sciences, under Award DE-SC0000989, and JZ by NSF award DMR-1611076.

ADDITIONAL NOTE

[a]In LJ units, LAMMPS sets the fundamental quantities mass m, length σ, energy ϵ, and the Boltzmann constant k_B equal to 1.

REFERENCES

(1) Fritzmann, C.; Löwenberg, J.; Wintgens, T.; Melin, T. State-of-the-art of reverse osmosis desalination. *Desalination* **2007**, *216*, 1−76.
(2) Strathmann, H. Electrodialysis, a mature technology with a multitude of new applications. *Desalination* **2010**, *264*, 268−288.
(3) Heuer, A.; Fink, D.; Laraia, V.; Arias, J.; Calvert, P.; Kendall, K.; Messing, G.; Blackwell, J.; Rieke, P.; Thompson, D.; et al. Innovative materials processing strategies: a biomimetic approach. *Science* **1992**, *255*, 1098.
(4) Shahinpoor, M. Ionic polymer-conductor composites as biomimetic sensors, robotic actuators and artificial muscles-a review. *Electrochim. Acta* **2003**, *48*, 2343−2353.
(5) Kazanskii, K.; Dubrovskii, S. *Polyelectrolytes Hydrogels Chromatographic Materials*; Springer: 1992; pp 97−133.
(6) Eichenbaum, G. M.; Kiser, P. F.; Dobrynin, A. V.; Simon, S. A.; Needham, D. Investigation of the Swelling Response and Loading of Ionic Microgels with Drugs and Proteins: The Dependence on Cross-Link Density. *Macromolecules* **1999**, *32*, 4867−4878.
(7) Keplinger, C.; Sun, J.-Y.; Foo, C. C.; Rothemund, P.; Whitesides, G. M.; Suo, Z. Stretchable, transparent, ionic conductors. *Science* **2013**, *341*, 984−987.
(8) Ono, T.; Sugimoto, T.; Shinkai, S.; Sada, K. Lipophilic polyelectrolyte gels as super-absorbent polymers for nonpolar organic solvents. *Nat. Mater.* **2007**, *6*, 429−433.
(9) Schreyer, H. B.; Gebhart, N.; Kim, K. J.; Shahinpoor, M. Electrical Activation of Artificial Muscles Containing Polyacrylonitrile Gel Fibers. *Biomacromolecules* **2000**, *1*, 642−647.
(10) Kim, H. I.; Park, S. J.; Kim, S. I.; Kim, N. G.; Kim, S. J. Electroactive polymer hydrogels composed of polyacrylic acid and poly(vinyl sulfonic acid) copolymer for application of biomaterial. *Synth. Met.* **2005**, *155*, 674−676.
(11) Kwon, H.-K.; Zwanikken, J. W.; Shull, K. R.; Olvera de la Cruz, M. Theoretical Analysis of Multiple Phase Coexistence in Polyelectrolyte Blends. *Macromolecules* **2015**, *48*, 6008−6015.
(12) Karnik, R.; Fan, R.; Yue, M.; Li, D.; Yang, P.; Majumdar, A. Electrostatic control of ions and molecules in nanofluidic transistors. *Nano Lett.* **2005**, *5*, 943−948.
(13) Cayre, O. J.; Chang, S. T.; Velev, O. D. Polyelectrolyte diode: nonlinear current response of a junction between aqueous ionic gels. *J. Am. Chem. Soc.* **2007**, *129*, 10801−10806.
(14) Koo, H.-J.; Chang, S. T.; Velev, O. D. Ion-Current Diode with Aqueous Gel/SiO_2 Nanofilm Interfaces. *Small* **2010**, *6*, 1393−1397.
(15) Fan, R.; Huh, S.; Yan, R.; Arnold, J.; Yang, P. Gated proton transport in aligned mesoporous silica films. *Nat. Mater.* **2008**, *7*, 303−307.
(16) Daiguji, H.; Yang, P.; Majumdar, A. Ion transport in nanofluidic channels. *Nano Lett.* **2004**, *4*, 137−142.
(17) Nam, S.-W.; Rooks, M. J.; Kim, K.-B.; Rossnagel, S. M. Ionic field effect transistors with sub-10 nm multiple nanopores. *Nano Lett.* **2009**, *9*, 2044−2048.
(18) Boon, N.; Olvera de la Cruz, M. Soft amplifier circuits based on field-effect ionic transistors. *Soft Matter* **2015**, *11*, 4793−4798.
(19) Yang, C. H.; Chen, B.; Lu, J. J.; Yang, J. H.; Zhou, J.; Chen, Y. M.; Suo, Z. Ionic cable. *Extreme Mechanics Letters* **2015**, *3*, 59−65.
(20) Gong, J. P.; Komatsu, N.; Nitta, T.; Osada, Y. Electrical Conductance of Polyelectrolyte Gels. *J. Phys. Chem. B* **1997**, *101*, 740−745.
(21) Travas-Sejdic, J.; Steiner, R.; Desilvestro, J.; Pickering, P. Ion conductivity of novel polyelectrolyte gels for secondary lithium-ion polymer batteries. *Electrochim. Acta* **2001**, *46*, 1461−1466.

DOI: 10.1021/acs.macromol.6b01276
Macromolecules XXXX, XXX, XXX−XXX

(22) Forsyth, M.; Sun, J.; Zhou, F.; MacFarlane, D. Enhancement of ion dissociation in polyelectrolyte gels. *Electrochim. Acta* **2003**, *48*, 2129−2136.
(23) Kidd, B. E.; Forbey, S. J.; Steuber, F. W.; Moore, R. B.; Madsen, L. A. Multiscale Lithium and Counterion Transport in an Electrospun Polymer-Gel Electrolyte. *Macromolecules* **2015**, *48*, 4481−4490.
(24) Pissis, P.; Kyritsis, A. Electrical conductivity studies in hydrogels. *Solid State Ionics* **1997**, *97*, 105−113.
(25) Colby, R. H.; Boris, D. C.; Krause, W. E.; Tan, J. S. Polyelectrolyte conductivity. *J. Polym. Sci., Part B: Polym. Phys.* **1997**, *35*, 2951−2960.
(26) Manning, G. S. Limiting laws and counterion condensation in polyelectrolyte solutions I. Colligative properties. *J. Chem. Phys.* **1969**, *51*, 924−933.
(27) Hall, C. C.; Zhou, C.; Danielsen, S. P.; Lodge, T. P. Formation of Multicompartment Ion Gels by Stepwise Self-Assembly of a Thermoresponsive ABC Triblock Terpolymer in an Ionic Liquid. *Macromolecules* **2016**, *49*, 2298−2306.
(28) Moon, H. C.; Kim, C.-H.; Lodge, T. P.; Frisbie, C. D. Multicolored, Low-Power, Flexible Electrochromic Devices Based on Ion Gels. *ACS Appl. Mater. Interfaces* **2016**, *8*, 6252−6260.
(29) Kitazawa, Y.; Ueki, T.; McIntosh, L. D.; Tamura, S.; Niitsuma, K.; Imaizumi, S.; Lodge, T. P.; Watanabe, M. Hierarchical Sol-Gel Transition Induced by Thermosensitive Self-Assembly of an ABC Triblock Polymer in an Ionic Liquid. *Macromolecules* **2016**, *49*, 1414−1423.
(30) Moon, H. C.; Lodge, T. P.; Frisbie, C. D. Electrochemiluminescent displays based on ion gels: correlation between device performance and choice of electrolyte. *J. Mater. Chem. C* **2016**, *4*, 8448−8453.
(31) Yan, Q.; de Pablo, J. J. Monte Carlo Simulation of a Coarse-Grained Model of Polyelectrolyte Networks. *Phys. Rev. Lett.* **2003**, *91*, 018301.
(32) Akerlof, G. Dielectric constants of some organic solvent-water mixtures at various temperatures. *J. Am. Chem. Soc.* **1932**, *54*, 4125.
(33) Plimpton, S.; Pollock, R.; Stevens, M. Particle-Mesh Ewald and rRESPA for Parallel Molecular Dynamics Simulations. *PPSC* **1997**, not-supplied.
(34) Jha, P. K.; Sknepnek, R.; Guerrero-Garcia, G. I.; Olvera de la Cruz, M. A graphics processing unit implementation of coulomb interaction in molecular dynamics. *J. Chem. Theory Comput.* **2010**, *6*, 3058−3065.
(35) Mann, B. A.; Holm, C.; Kremer, K. Swelling of polyelectrolyte networks. *J. Chem. Phys.* **2005**, *122*, 154903.
(36) Plimpton, S. Fast Parallel Algorithms for Short-Range Molecular Dynamics. *J. Comput. Phys.* **1995**, *117*, 1−19.
(37) Hünenberger, P. H. In *Advanced Computer Simulation: Approaches for Soft Matter Sciences I*; Holm, C., Kremer, K., Eds.; Springer: Berlin, 2005; pp 105−149.
(38) Halverson, J. D.; Lee, W. B.; Grest, G. S.; Grosberg, A. Y.; Kremer, K. Molecular dynamics simulation study of nonconcatenated ring polymers in a melt. I. Statics. *J. Chem. Phys.* **2011**, *134*, 204904.
(39) Frenkel, D.; Smit, B. *Understanding Molecular Simulation: From Algorithms to Applications*; Academic Press: 2001; Vol. *1*.
(40) Flyvbjerg, H.; Petersen, H. G. Error estimates on averages of correlated data. *J. Chem. Phys.* **1989**, *91*, 461−466.
(41) Khokhlov, A.; Starodubtzev, S.; Vasilevskaya, V. In *Responsive Gels: Vol. Transitions I*; Dušek, K., Ed.; Advances in Polymer Science; Springer: Berlin, 1993; Vol. *109*, pp 123−171.
(42) Donnan, F. G. The theory of membrane equilibria. *Chem. Rev.* **1924**, *1*, 73−90.
(43) Katchalsky, A.; Lifson, S.; Exsenberg, H. Equation of swelling for polyelectrolyte gels. *J. Polym. Sci.* **1951**, *7*, 571−574.
(44) Erbaş, A.; Olvera de la Cruz, M. Energy Conversion in Polyelectrolyte Hydrogels. *ACS Macro Lett.* **2015**, *4*, 857−861.
(45) Grass, K.; Holm, C. Polyelectrolytes in electric fields: measuring the dynamical effective charge and effective friction. *Soft Matter* **2009**, *5*, 2079−2092.
(46) Oosawa, F. *Polyelectrolytes*; Marcel Dekker: 1971.
(47) Deserno, M.; Holm, C.; May, S. Fraction of condensed counterions around a charged rod: Comparison of Poisson-Boltzmann theory and computer simulations. *Macromolecules* **2000**, *33*, 199−206.
(48) Deserno, M.; Holm, C. Theory and simulations of rigid polyelectrolytes. *Mol. Phys.* **2002**, *100*, 2941−2956.
(49) Netz, R. R. Nonequilibrium Unfolding of Polyelectrolyte Condensates in Electric Fields. *Phys. Rev. Lett.* **2003**, *90*, 128104.
(50) Jha, P. K.; Zwanikken, J. W.; Detcheverry, F. A.; de Pablo, J. J.; Olvera de la Cruz, M. Study of volume phase transitions in polymeric nanogels by theoretically informed coarse-grained simulations. *Soft Matter* **2011**, *7*, 5965−5975.
(51) Rumyantsev, A. M.; Pan, A.; Ghosh Roy, S.; De, P.; Kramarenko, E. Y. Polyelectrolyte Gel Swelling and Conductivity vs Counterion Type, Cross-Linking Density, and Solvent Polarity. *Macromolecules* **2016**, *49*, 6630.
(52) Quesada-Pérez, M.; Adroher-Benítez, I.; Maroto-Centeno, J. A. Size-exclusion partitioning of neutral solutes in crosslinked polymer networks: A Monte Carlo simulation study. *J. Chem. Phys.* **2014**, *140*, 204910.
(53) Yan, Q.; de Pablo, J. J. Phase Equilibria of Size-Asymmetric Primitive Model Electrolytes. *Phys. Rev. Lett.* **2001**, *86*, 2054−2057.
(54) Dufrêche, J.-F.; Jardat, M.; Turq, P.; Bagchi, B. Electrostatic relaxation and hydrodynamic interactions for self-diffusion of ions in electrolyte solutions. *J. Phys. Chem. B* **2008**, *112*, 10264−10271.

DOI: 10.1021/acs.macromol.6b01276
Macromolecules XXXX, XXX, XXX−XXX